Materials Transactions, Vol. 59, No. 11 (2018) pp. 1845 to 1853

High-Temperature Stability of $ThMn_{12}$ Magnet Materials

Kurima Kobayashi[1,*1], Daiki Furusawa[1], Shunji Suzuki[1], Tomoko Kuno[1,2,*2], Kimiko Urushibata[1], Noritsugu Sakuma[3,4], Masao Yano[3,4], Tetsuya Shoji[3,4], Akira Kato[3,4], Akira Manabe[4] and Satoshi Sugimoto[2]

[1]*Department of Materials and Life Science, Shizuoka Institute of Science and Technology, Fukuroi 437-8555, Japan*
[2]*Department of Materials Science, Graduate School of Engineering, Tohoku University, Sendai 980-8579, Japan*
[3]*Toyota Motor Corporation, Susono 410-1193, Japan*
[4]*Technology Research Association of Magnetic Materials for High-efficiency Motors (MagHEM) Higashifuji Branch, Susono 410-1193, Japan*

The nitrogenated alloys $(Nd_{0.7}Zr_{0.3})(Fe_{0.75}Co_{0.25})_{11.5}Ti_{0.5}N_{1.3}$ (A) and $Nd(Fe_{0.8}Co_{0.2})_{11}Mo_{1.0}N_{1.0}$ (B) and the non-nitrogenated alloy $(Sm_{0.8}Zr_{0.2})(Fe_{0.75}Co_{0.25})_{11.5}Ti_{0.5}$ (C), having a $ThMn_{12}$ structure, show interesting magnetic properties and are candidate materials for high-temperature magnets. In this study, the stability of these materials was studied using Curie temperature measurements, differential scanning calorimetry, differential thermal analysis, thermogravimetry from room temperature to 1573 K, and X-ray diffraction of treated samples. The nitrogenated samples (A) and (B) started to decompose into the α-(Fe, Co) phase and other X-ray amorphous phases from about 800 and 1000 K, respectively. Sample (C) exists as a metastable phase at room temperature and decomposed above 700 K at a relatively high oxygen partial pressure ($P_{O2} > 10$ Pa), but the $ThMn_{12}$ structure remained up to at least 1373 K in an almost oxygen-free atmosphere ($P_{O2} < 10^{-15}$ Pa). Sample (C) is intrinsically stable at temperatures higher than about 1000 K up to the melting temperature, which was estimated to be 1480 K. The $ThMn_{12}$ structure in both R = Nd and Sm starting alloys is metastable at room temperature, and becomes unstable under 800–1000 K. The decomposition rate was clearly dependent on the P_{O2} in the heated atmosphere, as high P_{O2} led to sample oxidation, and on the sample composition. [doi:10.2320/matertrans.M2018195]

(Received June 12, 2018; Accepted August 6, 2018; Published October 25, 2018)

Keywords: *1-12 structure compounds, high-temperature stability, polarization change by heating, differential thermal analysis and thermogravimetry analysis, differential scanning calorimetry analysis, high-temperature X-ray diffraction, oxygen partial pressure*

1. Introduction

Since the 1980s, magnetic materials with a $ThMn_{12}$ structure have attracted interest because of the high Fe concentration in the unit cell, which means that the saturation polarization of these materials is higher than those of 1-5, 1-7, and 2-17 compounds. The ternary and plural alloys of R–(Fe, Co)–transition metal (TM) (R = Nd, Sm; TM = Ti, Mo, V, Si) with Th_2Zn_{17}, Th_2Ni_{17}, $ThMn_{12}$, and other (Fe, Co)-rich (+TM) structures have been investigated as candidate compounds for permanent magnet materials.[1,2] The 2-17 structures can be stabilized without a third TM element, whereas the 1-12 structures require the TM.[1,2] Therefore, the 1-12 compounds investigated in previous studies had compositions of $R(Fe, Co)_{12-y}TM_y$ ($y > 1.0$). A TM element ($y > 1.0$) was required to stabilize the $ThMn_{12}$ structure.

In our previous studies, we investigated elemental substitution, including substituting Co into Fe sites and Zr into R sites, in the 1-12 compounds based on the atomic size.[3,4] With respect to the magnetic properties, we showed that the nitrogenated R = Nd compound $(Nd_{0.7}Zr_{0.3})(Fe_{0.75}Co_{0.25})_{11.5}Ti_{0.5}N_{1.30}$ had good magnetic properties of $J_s = 1.67$ T and $H_a = 5.25$ MA/m at room temperature (RT). The R = Sm alloy, $(Sm_{0.8}Zr_{0.2})(Fe_{0.75}Co_{0.25})_{11.5}Ti_{0.5}$, also had $J_s = 1.58$ T and $H_a = 5.90$ MA/m at RT. The values for the R = Sm alloy were still $J_s = 1.50$ T and $H_a = 3.70$ MA/m at 473 K, and were higher than those of the $Nd_2Fe_{14}B$ phase at this temperature.[5–7] Because the R = Sm alloy is a Dy-free and N-free powder, it is a promising candidate for sintered magnets. We also investigated the site occupation of Nd (and Sm), Ti, Zr, and Co in the $ThMn_{12}$ structure of these compounds using Cs-corrected scanning transmission electron microscopy and revealed the presence of Ti-, Co- and Zr-substituted sites in the $ThMn_{12}$ structure.[8–10]

Materials for permanent magnets must also be stable at high temperatures, in addition to having high values of J_s, H_a, and T_C. The R = Nd compounds must be nitrogenated to obtain high magnetic anisotropy; however, nitrogenated compounds decompose into other phases at comparatively low temperatures of 800–1000 K, similar to $Sm_2Fe_{17}N_3$ compounds.

Furthermore, conventional magnet powders are typically sintered at temperatures higher than 1300 K; thus, the compounds must be stable in this temperature region. Therefore, it should be emphasized that high-temperature stability is important for both nitrogenated R = Nd compounds with a $ThMn_{12}$ structure and non-nitrogenated R = Sm compounds that are candidate materials for sintered magnets.

Concerning the stability of related compounds, we already partially reported the variations of J_s and H_a with increasing temperature for the compounds described in Refs. 3) and 5). Raghavan reported phase diagrams for the Sm–Fe–Ti system and suggested that the $ThMn_{12}$ structure in the three-component system is unstable at around 873 K.[11] Recently, Hirayama *et al.*[12] published the temperature dependence of magnetic properties, such as J_s and H_a, in Sm $(Fe_{1-x}, Co_x)_{12}$ and other related alloys and nitrides.

In this paper, we studied the high-temperature (mainly 700–1373 K) stability of three typical 1-12 compounds, the nitrogenated alloys $(Nd_{0.7}Zr_{0.3})(Fe_{0.75}Co_{0.25})_{11.5}Ti_{0.5}N_{1.2}$ (note

*[1]Corresponding author, E-mail: kobayashi.kurima@sist.ac.jp
*[2]Graduate Student, Tohoku University

Table 1 Compositions, lattice constants, unit cell volumes, and magnetic properties of the samples at RT.

Sample	*Lattice constant*				α-Fe /vol %	*Saturation Polarization,* J_s / T	*Anisotropy Field,* H_a / (MA/m)
	a / nm	*c* / nm	*(c/a)* / %	*V* / nm^3			
(A) $(Nd_{0.7}Zr_{0.3})(Fe_{0.75}Co_{0.25})_{11.5}Ti_{0.5}N_{1.2}$	0.862	0.484	56.14	0.360	16.7	1.67	5.25
(B) $Nd(Fe_{0.8}Co_{0.2})_{11.0}MoN_{1.0}$	0.864	0.485	56.13	0.362	0.2	1.35	6.68
(C) $(Sm_{0.8}Zr_{0.2})(Fe_{0.75}Co_{0.25})_{11.5}Ti_{0.5}$	0.851	0.477	56.05	0.346	6.4	1.58	5.90

that this is different from the $-N_{1.3}$ compound discussed in Ref. 3)) and $Nd(Fe_{0.8}Co_{0.2})_{11}Mo_{1.0}N_{1.0}$, and the non-nitrogenated alloy $(Sm_{0.8}Zr_{0.2})(Fe_{0.75}Co_{0.25})_{11.5}Ti_{0.5}$. The two nitrogenated compounds were selected because the former ($-Ti_{0.5}N_{1.2}$) exhibits good magnetic properties and the latter ($-Mo_{1.0}N_{1.0}$) is stable up to about 1000 K and exhibits the highest thermal stability of the 1-12 nitrogenated compounds studied in our experiments. The third R = Sm alloy was selected for its good magnetic properties at high temperatures[5] and the likelihood that it could be sintered at 1350–1450 K.

We investigated the stability by using polarization measurements as a function of temperature, high-temperature X-ray diffraction (XRD), ordinary XRD at RT after heat treatment at 673–1373 K, differential scanning calorimetry (DSC), and differential thermal analysis and thermogravimetry (DTA-TG). We also used a stabilized ZrO_2 ceramic oxygen sensor and pump for controlling oxygen partial pressure (P_{O2}) during the high-temperature treatment.

2. Experimental and Results

2.1 Sample preparation

We prepared nitrogenated samples (A) ($(Nd_{0.7}Zr_{0.3})(Fe_{0.75}Co_{0.25})_{11.5}Ti_{0.5}N_{1.2}$) and (B) ($Nd(Fe_{0.8}Co_{0.2})_{11}Mo_{1.0}N_{1.0}$) and non-nitrogenated sample (C) ($(Sm_{0.8}Zr_{0.2})(Fe_{0.75}Co_{0.25})_{11.5}Ti_{0.5}$). The processing of the alloys was the same as that in our previous studies.[3,5,8–10] The alloys were annealed under optimum conditions, at 1473 K (sample (A)) and at 1373 K (samples (B) and (C)), for 4 h in an Ar atmosphere. Samples (A) and (B) were nitrogenated at 723 and 873 K, respectively, for 4 h in a N_2 atmosphere. Sample (A) was similar to that in our previous papers; in particular, the lattice constants and magnetic properties were similar to those in Ref. 3) ($-N_{1.3}$). Before nitrogenation of samples (A) and (B), the powders were pulverized to a diameter of less than 30 μm using a cutter mill. The average diameters (D_{AV}) of the obtained powders including sample (C) were about 20–25 μm according to SEM observations.

Table 1 shows the lattice constants (*a* and *c*) and crystal parameters, the amount of α-(Fe, Co) phase, saturation polarization (J_s), and anisotropy field $\mu(H_a)$, which were measured with a vibrating-sample magnetometer (VSM) and the law of approach to magnetic saturation (LAS).

Samples (A) and (C) showed excellent magnetic properties. Sample (B), which contained $-Mo_{1.0}$, had a comparatively low saturation polarization ($J_s = 1.35$ T) and a high magnetic anisotropy field ($H_a = 6.68$ MA/m). The J_s values of samples (A) and (C) in Table 1 were corrected using the volume fractions of the α-(Fe, Co) phase ($J_s \approx 2.2$ T). The values, therefore, correspond to those of the 1-12 phases in the samples. The nitrogen contents of the samples, (A) and (B), were controlled to about $-N_{1.0}$ with nitrogenation in a N_2 atmosphere.

In this study, the α-(Fe, Co) phase contents were measured using the following method.

As shown in Fig. 1, grains with the 1-12 structure (Fig. 1(a)) and micrometer-sized grains of the α-(Fe, Co) phase (Fig. 1(b)) are distinguishable using the electron backscattering diffraction (EBSD) method. Figure 1 shows the case of a particle of sample (A), in which the volume fraction of the α-(Fe, Co) phase is 16.7%. It is possible to determine the volume fraction of the α-(Fe, Co) phase from the images shown in Fig. 1. The two-dimensional surface area of the α-(Fe, Co) phase determined by EBSD is directly related to the volume fraction of the phase.[13] For the identification of the 1-12 and α-(Fe, Co) phases, we used crystal structure information for the $NdFe_{11}Ti$ and α-Fe phases, respectively.

It is necessary to know the relationship between the precipitated volume fraction of the α-(Fe, Co) phase by EBSD and the ratios of the XRD intensities of the (110) peak of the α-Fe phase to the (321) and (400) peaks of the 1-12 phase. The actual observed XRD patterns of the samples will be presented later during the discussion of the high-temperature XRD measurements. The transfer factor between the values (vol%) based on the EBSD results and the XRD peak intensity ratios were found to be about 0.3 in our previous studies, which was determined from the independent data obtained for four samples and confirmed by EBSD observations of other samples with a similar $ThMn_{12}$ structure.[3] That is to say, a value of 19.2% from the XRD

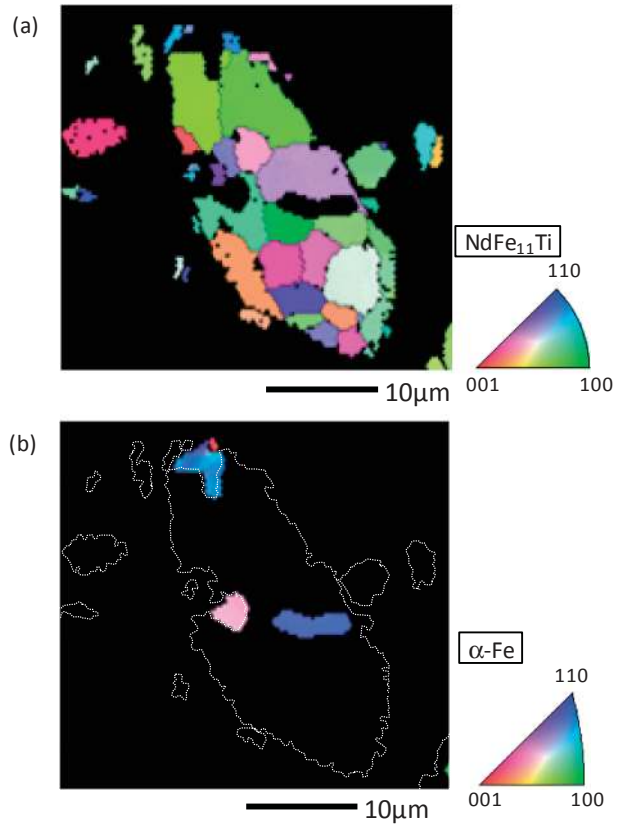

Fig. 1 EBSD images of the grains with (a) $ThMn_{12}$ structure and (b) α-Fe structure in a particle of sample (A).

peak intensity ratio $(110)_{Fe}/(321)_{1\text{-}12}$ corresponded to about 6.4% in the EBSD observations, that is, the volume fraction in the case of sample (C). However, we only use the directly transferred ratios from XRD intensities shown in Table 1 in this study.

Although the volume fraction was the same, the intensity of the $(110)_{Fe}$ peak in the α-(Fe, Co) phase is greater than those of the $(321)_{1\text{-}12}$ and $(400)_{1\text{-}12}$ peaks of the 1-12 phase, because of the difference in the original structure factor and the crystallinity of the phase. The volume fraction of the α-(Fe, Co) phase may be proportional to the XRD intensity of the phase, but the proportionality constant between the fraction and the intensity is different from those for the 1-12 phase. This is believed to explain the origin of the above transfer factor of 0.3.

It should be emphasized that even for the sample with the highest content of the α-(Fe, Co) phase, that is, sample (A), the separation between the 1-12 phase grains and the α-(Fe, Co) phase was very clear, as shown in Fig. 1, and no grains of mixed composition or an intermediate amorphous phase were observed.

2.2 Temperature dependence of saturation polarization

Figure 2 shows the temperature dependence of the saturation polarization (J_s) under applied field of 15 T for the samples obtained in this study. The measurements were performed using a VSM at the High Field Laboratory for Superconducting Materials of the Institute for Materials Research at Tohoku University in a 15 T magnetic field. The saturation polarizations of samples (A) and (C) showed

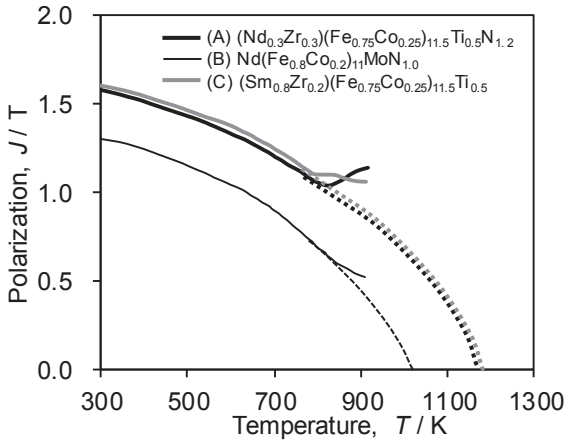

Fig. 2 Temperature dependence of the saturation polarization for the three samples examined in this study. Solid lines represent the measured polarization and dashed lines represent the extrapolated data.

obvious deviation from the extrapolated curves from about 800 K. This deviation, however, occurred at the slightly higher temperature of approximately 830 K for sample (B).

For samples (A) and (B), the decomposition of the compounds in this temperature region was ascribed to the loss of nitrogen from the structure, whereas the decomposition of sample (C) was attributed to the instability of the $ThMn_{12}$ structure.[11)]

The extrapolated Curie temperatures of the samples without the decomposition of the 1-12 phase were estimated to be about 1170 K for samples (A) and (C) and about 1000 K for the Nd(–Mo) system 1-12 compound, sample (B).

2.3 Thermal analyses of the prepared samples

DTA-TG measurements were performed with a thermal analyzer (TG-DTA2000SE, Netzsch). DSC was conducted on a differential scanning calorimeter (DSC403F3, Netzsch). In both measurements, heating rates were 10 K/min, data were obtained at intervals of 1 sec, and measurements were taken under an Ar atmosphere. However, the measurement chambers were not perfectly sealed and the oxygen partial pressure (P_{O2}) was estimated to be 10–100 Pa. During the measurements, the temperature was increased to 1573 K. Therefore, the samples were kept in a comparatively high P_{O2} atmosphere for a total of more than 150 min.

Figures 3(a) and (b) show the DSC and DTA curves, respectively, up to 1573 K for the samples. Sample (A), $(Nd_{0.7}Zr_{0.3})(Fe_{0.75}Co_{0.25})_{11.5}Ti_{0.5}N_{1.2}$, showed two peaks in both the DSC and DTA curves, although the peak intensities in the DSC curve were larger than those in the DTA curve. The first exothermic peak was at about 870 K and the second endothermic peak was at around 1300 K. The first exothermic peak is considered to correspond to the decomposition of the nitrogenated phase, and the second peak may be the Curie temperature and/or phase transition in the α-(Fe, Co) phase that appeared after the decomposition of the main 1-12 phase. The latter peak will be discussed in the Discussion section.

For sample (B), $Nd(Fe_{0.8}Co_{0.2})_{11}Mo_{1.0}N_{1.0}$, the first exothermic peak was detected at around 1050 K (Fig. 3(a)), approximately 200 K higher than that for sample (A). This exothermic peak is also considered to correspond to the

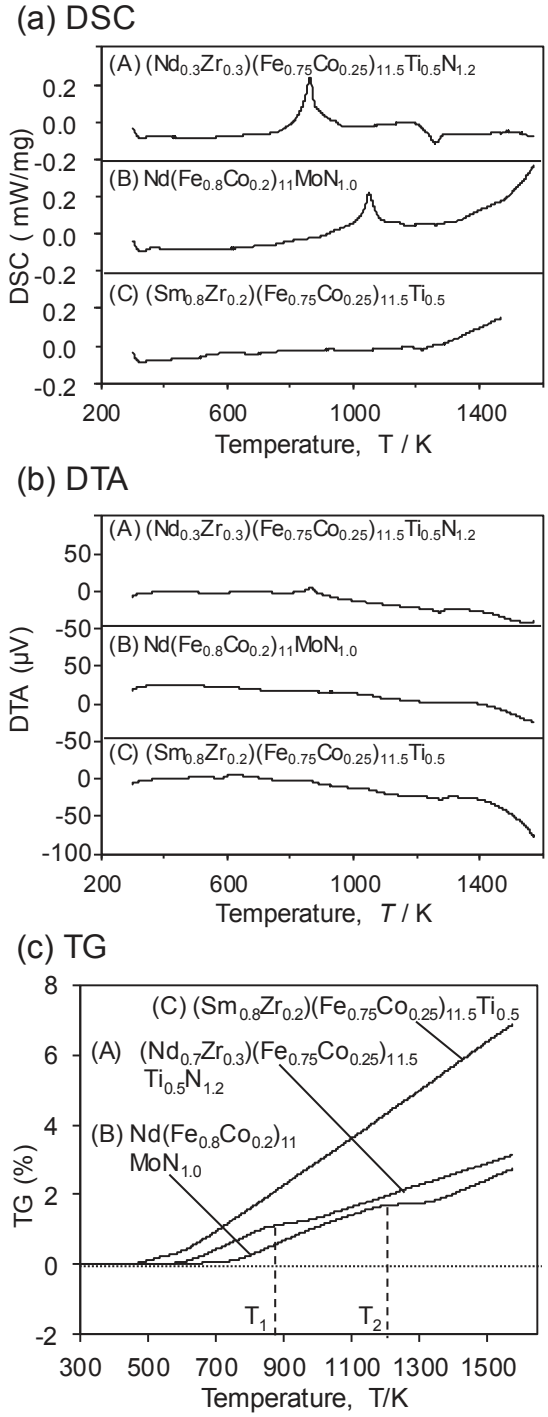

Fig. 3 Thermal analysis results: (a) DSC curves, (b) DTA curves, and (c) TG curves.

decomposition of the nitrogenated phase, and there was no clear peak in the higher temperature region. In the DTA curves shown in Fig. 3(b), the peaks are not so clear compared with the DSC curves. The decomposition mechanism for sample (B) appeared to be different from that for sample (A).

The non-nitrogenated sample (C), $(Sm_{0.8}Zr_{0.2})(Fe_{0.75}Co_{0.25})_{11.5}Ti_{0.5}$, showed no clear peaks up to about 1573 K, except for a small endothermic peak at around 1220 K in the DSC curve (Fig. 3(a)). The physical meaning of each peak observed in the DSC and DTA measurements shown in Fig. 3(a) and (b) will be explained later in the Discussion section.

Figure 3(c) shows the TG curves of the samples. The weight of sample (C) monotonously increased up to 1573 K, and the weight gain reached about 7% of the total sample weight. In contrast, the weight gains for samples (A) and (B) were about 2–3% even at 1573 K. A plateau in the weight increase was observed at around 850–950 K for sample (A) and at around 1100–1300 K for sample (B). These plateaus were attributed to nitrogen loss from the samples and decomposition of the $ThMn_{12}$ phase, as explained later in the Discussion section.

The total weight increases measured at RT after heating and cooling were 5.07% and 4.93% for samples (A) and (B), respectively. In contrast, the total weight of the non-nitrogenated sample (C) increased by 8.73% after heating and cooling. The weight gains of the nitrogenated samples (A) and (B) were clearly smaller than that of the non-nitrogenated R = Sm alloy, sample (C). Gas analysis revealed that the initial weight gain in sample (C) up to about 1000 K mainly arose from sample oxidation.

In the case of sample (C), samarium vaporization was also expected to occur at temperatures higher than about 1373 K. A high rate of Sm vaporization would be expected to result in a decrease in the weight gain in the high-temperature region of 1300–1573 K. However, the rate of weight gain observed in this region in Fig. 3(c) is similar to that in the lower temperature region.

2.4 X-ray diffraction patterns of the samples

XRD was conducted using an X-ray diffractometer (SmartLab, Rigaku, Japan). We used two XRD methods. High-temperature XRD (XRD-A) was performed under the following conditions in the XRD chamber: Co Kα, $\lambda =$ 0.1789 nm; slits, 2/3°-2/3°-0.6 mm; scanning speed, $2\theta =$ 1°/min; sampling, $\theta = 0.04°$; atmosphere, Ar (graphite cover; estimated $P_{O2} > 10$ Pa); heating rate, 20 K/min. The penetration depth of the X-rays (Co Kα) was estimated to be about 11 μm (similar to α-Fe). The measured sample was kept in the XRD chamber, and the pattern at each temperature was obtained within about 1 hour, $2\theta = 20$–80°. The temperature was increased in a stepwise manner at intervals of 200 K from RT to 1273 K. It should be mentioned that XRD in this method (XRD-A) was detected through the graphite window of the instrument.

XRD at RT (XRD-B) was conducted under the following conditions: Cu Kα, $\lambda = 0.1542$ nm; scanning speed, $2\theta =$ 5°/min; sampling, $\theta = 0.1°$ at RT. The heat treatment of the sample was conducted at each temperature for about 1 h in Ar ($P_{O2} \approx 10^{-2}$ Pa) atmosphere. The heating rate was 10 K/min from RT. The XRD pattern measurements were performed at RT after cooling, in air.

Figure 4(a) shows the XRD patterns for sample (A) ($(Nd_{0.7}Zr_{0.3})(Fe_{0.75}Co_{0.25})_{11.5}Ti_{0.5}N_{1.2}$). The peaks at around $\theta = 51.8°$ (Fig. 4(a) XRD-A, Co Kα) and $\theta = 44.5°$ (Fig. 4(a), XRD-B, Cu Kα) were attributed to the precipitated α-(Fe, Co) phase. XRD data from the International Center for Diffraction Data (ICDD) for $NdFe_{11}Ti$ (Card No. 01-078-9757) are shown at the bottom of Fig. 4(a) for XRD-A (Co Kα) and XRD-B (Cu Kα). These data consist of

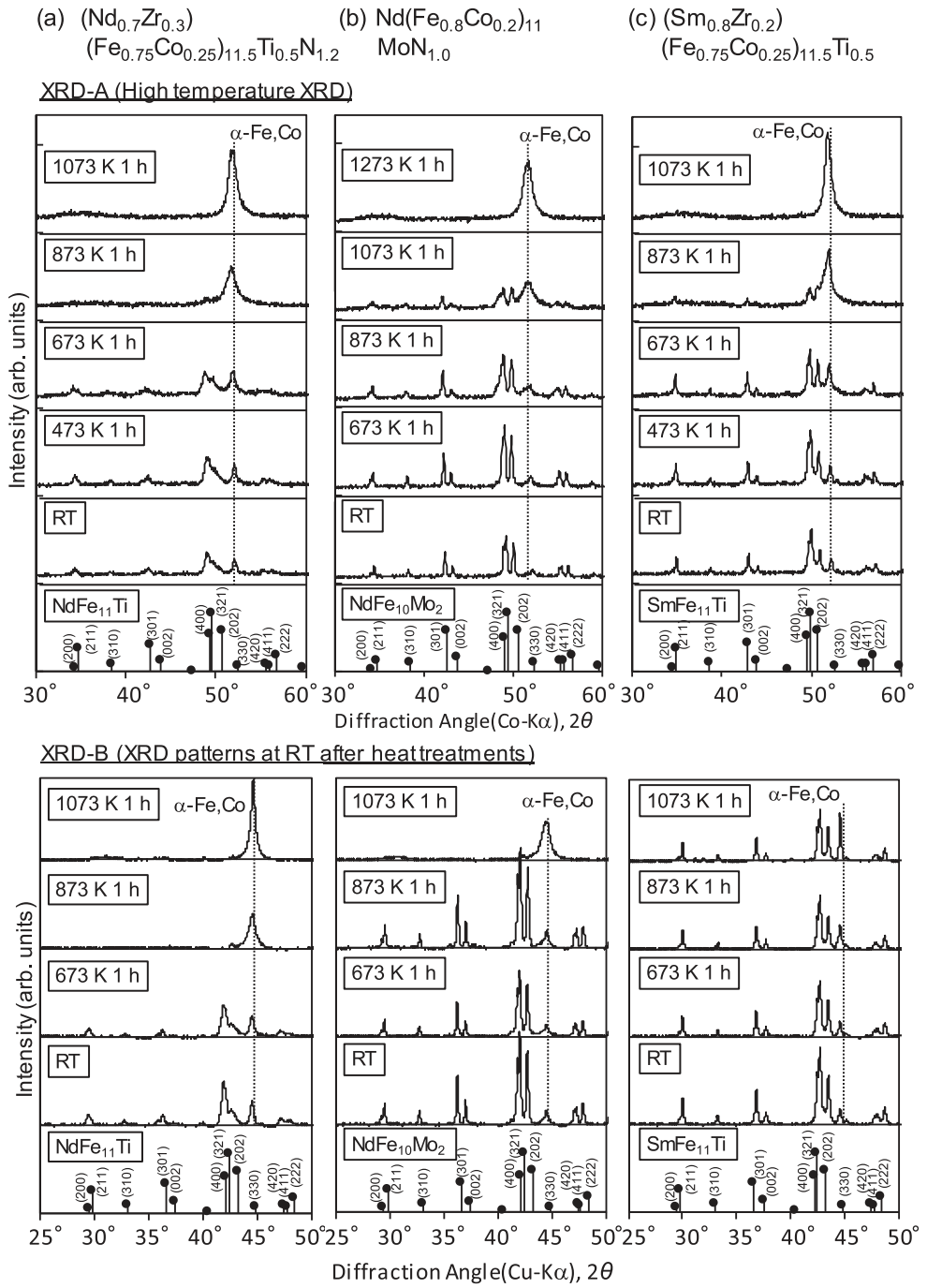

Fig. 4 High-temperature X-ray diffraction patterns of samples (A), (B), and (C). In XRD-A, the XRD patterns were measured at the indicated temperatures. In XRD-B, the XRD patterns were measured at RT after heat treatment at the indicated temperatures.

only the 2θ values and relative intensities of the diffraction peaks; therefore, we show only the vertical data lines in Fig. 4(a) and subsequent figures.

The measured XRD patterns show a slight decrease in the diffraction angles compared with those of the ICDD standard pattern of the $NdFe_{11}Ti$ phase. The main reason for this shift is considered to be lattice expansion in the prepared sample (A) due to nitrogenation ($-N_{1.2}$). Our motivation for showing the ICDD pattern of the $NdFe_{11}Ti$ phase is to demonstrate the existence of a basic 1-12 structure in sample (A).

Figure 4(a) shows the XRD patterns at each temperature obtained by XRD-A. The original high-temperature XRD patterns were in the range $2\theta = 20$–$80°$. The sample was kept around each temperature for 60–70 min including the heating time. The $ThMn_{12}$ structure existed up to 673 K, but had disappeared at 873 K, and the precipitated α-(Fe, Co) phase gradually increased in the higher temperature region. The XRD peak heights in the XRD-A patterns were lower than those in the XRD-B patterns, because of instrumental limitations (graphite window) and the mixture of crystal information from the surface and center portions of the sample particles (using Co Kα).

The results obtained by XRD-B (Fig. 4(a), XRD-B) were similar to those obtained by XRD-A. However, the crystallinity of the main 1-12 phase seemed to be higher

by XRD-B up to 673 K. This suggests that the low P_{O2} of $\sim 10^{-2}$ Pa in the XRD-B heat-treatment atmosphere maintained the crystallinity of the 1-12 structure at the surface of the samples, up to the X-ray penetration depth of about 2 μm.

Figure 4(b) shows that sample (B) ($Nd(Fe_{0.8}Co_{0.2})_{11}$-$Mo_{1.0}N_{1.0}$) retained its 1-12 structure up to 873 K, which was about 200 K higher than for sample (A) ($-Ti_{0.5}N_{1.2}$). In the XRD patterns measured by the XRD-B method, the pattern of the 1-12 structure disappeared at 1073 K. However, for the XRD-A method, a weak 1-12 pattern was detected even in the pattern obtained at 1073 K. The XRD pattern reflects the surface structure to a depth of ~2 μm for XRD-B, but to a depth of 11 μm for XRD-A (Co Kα), which may explain why the residual 1-12 phase was detected. That is, the 1-12 structure at the center of sample particles remained up to about 1073 K. The main peak of the precipitated α-(Fe, Co) phase was weaker than that in the XRD patterns of sample (A).

In Fig. 4(b), the ICDD standard XRD pattern of $NdFe_{10}Mo_2$ (Card No. 01-071-8302) is shown as vertical lines below the patterns obtained by XRD-A and XRD-B. The main reason for the peak shift to lower angles is considered to be lattice expansion in the prepared sample (B) due to nitrogenation ($-N_{1.0}$). Our motivation for showing the ICDD pattern of the $NdFe_{10}Mo_2$ phase is to demonstrate the existence of a basic 1-12 structure in sample (B).

Figure 4(c) shows the results for sample (C) ($(Sm_{0.8}Zr_{0.2})(Fe_{0.75}Co_{0.25})_{11.5}Ti_{0.5}$), which were different from those for the nitrogenated samples (A) and (B). When XRD-A was used, the pattern of the 1-12 phase almost disappeared at 873 K, and only the main peak for the α-(Fe, Co) phase was observed at 1073 K (Fig. 4(c), XRD-A). In contrast, the XRD pattern of the 1-12 phase remained from RT to 1073 K when XRD-B was used (Fig. 4(c), XRD-B). The main peak of the α-(Fe, Co) phase gradually became stronger as the treatment temperature was increased.

The XRD-A and XRD-B results seem to contradict each other, because the temperature stability of the 1-12 phase should be identical even when using different XRD methods. The obvious difference between XRD-A and XRD-B is the P_{O2} of the measuring atmosphere, which was estimated to be $P_{O2} \approx 10$ Pa for XRD-A and measured as $P_{O2} = 10^{-2}$ Pa for XRD-B (using a P_{O2} sensor). This difference originated from the differences between the sealing of the chamber (XRD-A) and that of the ceramic tube in which oxygen was eliminated using ZrO_2 ceramic pump in the furnace (XRD-B). It should also be considered that sample (C) is poorly resistant to oxidation, as shown in Fig. 3(c). The disappearance of the 1-12 structure above 873 K in XRD-A may be caused by oxidation of the sample. In fact, this structure existed up to 1073 K at a low P_{O2} of 10^{-2} Pa in XRD-B. This point will be addressed in more detail in the discussion of Fig. 5.

In Fig. 4(c), we show the ICDD pattern for the $SmFe_{11}Ti$ (Card No. 03-065-5363) phase to demonstrate the existence of a basic 1-12 structure in sample (C) at each treatment temperature.

As described in Section 2.3 and shown in Fig. 3(c), the weight gain caused by oxidation was larger for sample (C) (~7% up to 1573 K) than for the nitrogenated samples (A) and (B) (~3% up to 1573 K). Therefore, the results in Fig. 4(c) are considered to arise from sample oxidation as we mentioned above.

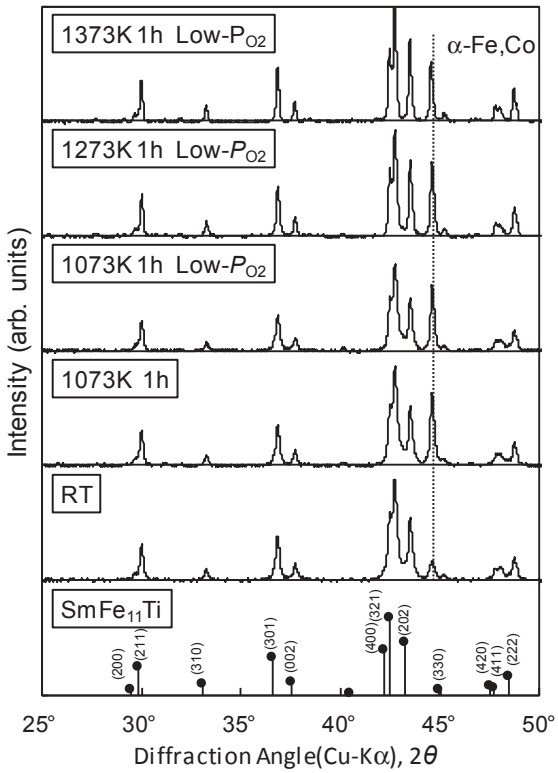

Fig. 5 XRD patterns observed by XRD-B for sample (C) ($(Sm_{0.8}Zr_{0.2})$-$(Fe_{0.75}Co_{0.25})_{11.5}Ti_{0.5}$). The atmosphere during heat treatment was controlled and measured using a ZrO_2 ceramic oxygen pump and sensor, respectively.

We examined the effect of oxidation, which causes the decomposition of sample (C) (appearance of the α-(Fe, Co) phase), on the stability of the 1-12 phase. We compared the samples heated at 1073 K in Ar ($P_{O2} = 10^{-2}$ Pa) as shown in Fig. 4(c) and in Ar with oxygen removed using a ZrO_2 ceramic oxygen pump ($P_{O2} = 10^{-15}$ Pa; Low-P_{O2}) (Fig. 5; 1073 K 1 h and 1073 K 1 h Low-P_{O2}). In addition, the temperature was increased to 1273 K or 1373 K in the latter atmosphere with oxygen removed ($P_{O2} = 10^{-15}$ Pa; Low-P_{O2}) (Fig. 5; 1273 K 1 h Low-P_{O2} and 1373 K 1 h Low-P_{O2}).

The intensities of the strongest peak of the α-(Fe, Co) phase at about $2\theta = 44.5°$ with Cu Kα diffraction were similar for the three samples treated at 1073 K and 1273 K in both Ar atmospheres ($P_{O2} = 10^{-2}$ Pa and $P_{O2} = 10^{-15}$ Pa; Low-P_{O2}), as shown in Fig. 5. The content of the α-(Fe, Co) phase in the samples was evaluated to be about 22–25 vol% based on the XRD peak intensity ratio $(110)_{Fe}/(321)_{1\text{-}12}$.

In the figure, the XRD pattern of a sample treated at 1373 K for 1 h in $P_{O2} = 10^{-15}$ Pa (1373 K 1 h Low-PO_2) is also shown. For the heat treatment of this sample, the sample was rapidly inserted into and taken out from the isothermal zone of the furnace. Therefore, the duration of exposure to the 800–1000 K temperature range[11] was limited and obviously shorter than that of the other samples. Although the treatment temperature was increased to 1373 K, the intensity of the $(110)_{Fe}$ peak decreased and the content of the α-(Fe, Co) phase was evaluated as 17.5 vol%, which is

obviously smaller than that of the three previous samples treated at 1073 K or 1273 K.

Therefore, it was estimated that oxidation was not only reason for the decomposition of sample (C), that is, the appearance of the α-(Fe, Co) phase, during the 1073–1273 K treatments shown in Fig. 5. The heat treatment at 800–1000 K decreased the stability of the $ThMn_{12}$ structure,[11] and the decomposition reaction of the 1-12 structure should be accelerated at a comparatively high P_{O2} ($\sim$ 10 Pa) as in XRD-A (Fig. 4(c)). The (110) peak of α-(Fe, Co) at $2\theta \approx 44.5°$ in Fig. 5, therefore, was partially produced during heat treatment at 800–1000 K.

3. Discussion

We studied the thermal stability of samples (A) ($(Nd_{0.7}Zr_{0.3})(Fe_{0.75}Co_{0.25})_{11.5}Ti_{0.5}N_{1.2}$), (B) ($Nd(Fe_{0.8}Co_{0.2})_{11}Mo_{1.0}N_{1.0}$), and (C) ($(Sm_{0.8}Zr_{0.2})(Fe_{0.75}Co_{0.25})_{11.5}Ti_{0.5}$) (Table 1) at high temperatures. Samples (A) and (B) were nitrogenated to achieve high magnetic anisotropy. Nitrogenated compounds, such as $Sm_2Fe_{17}N_3$ and samples (A) and (B) in this study, ordinarily start to decompose into metal nitrides (RN_x) and iron-rich phases (e.g., α-(Fe, Co)) from about 800 K (Figs. 2, 3, and 4). Therefore, the preparation of sintered magnets is difficult using nitrogenated compounds.

At temperatures below the decomposition temperature, nitrogenation provides higher resistance to oxidation. The weight gain caused by oxidation of the nitrogenated samples (A) and (B) was about 5%, but that of non-nitrogenated sample (C) was about 9% after heating and cooling from RT to 1573 K in similar atmospheres in the DTA-TG and DSC instruments. During heating up to only 1573 K (Fig. 3(c)), the weight gain was about 3% for samples (A) and (B) and 7% for sample (C). Moreover, sample (C) decomposed readily in a high-P_{O2} atmosphere (estimated to be >10 Pa) at around 800 K, such as during XRD-A (Fig. 4(c)).

In contrast, the 1-12 structure in sample (C) was stable in the Ar atmosphere with a low P_{O2} of 10^{-15} Pa, up to the melting temperature, when oxygen was eliminated using a ZrO_2 oxygen pump. It should be emphasized that the XRD pattern of sample (C) (RT in Fig. 5) is that of a sample annealed at 1373 K for four hours in an Ar atmosphere (low P_{O2}). Thin alloy plates of 5–10 mm in diameter and about 500 μm thickness were annealed at 1373 K and then pulverized into particles of 20–30 μm diameter. The pulverized powder contains α-(Fe, Co) phase of about 6.4 vol% as shown in Table 1. All of the other heat-treated samples (Fig. 5, 1073 K 1 h to 1373 K 1 h Low-P_{O2}), however, were obtained by pulverizing the annealed plate sample into a powder with a particle diameter of 20–30 μm and then subjecting the powder to heat treatment at the stated temperature. The surface area, therefore, is obviously larger for the latter samples than for the initial annealed sample (C). The XRD patterns of the treated samples are shown in Figs. 4 and 5.

Another important characteristic of 1-12 compounds is that the $ThMn_{12}$ structure is stable at high temperatures above about 1100 K.[11] Therefore, the $ThMn_{12}$ structure observed by XRD at RT is a metastable phase. A characteristic phase appearing after decomposition is the α-(Fe, Co) phase described in this study. When sample (C) was heated in a high-P_{O2} atmosphere, the decomposition was accelerated (Fig. 4(c), XRD-A), although the $ThMn_{12}$ structure was clearly detected up to 1273 K in a low P_{O2} of $\sim 10^{-15}$ Pa. The 1-12 phase becomes more stable at 1373 K (Fig. 5) despite the appearance of the (110) peak of the α-(Fe, Co) phase as shown in Fig. 5.

The peak intensity ratios of the (110) peak of the α-Fe phase to the (321) and (400) peaks of the 1-12 phase are shown in Fig. 6. The differences between the peak shapes for sample (A) and those for samples (B) and (C) are considered to originate from the inhomogeneity of the nitrogen concentration in particles of sample (A). Moreover, Co Kα X-rays were used in XRD-A but Cu Kα X-rays were used in XRD-B; the corresponding X-ray penetration depths are about 11 μm and 2 μm, respectively, in the case of the α-Fe

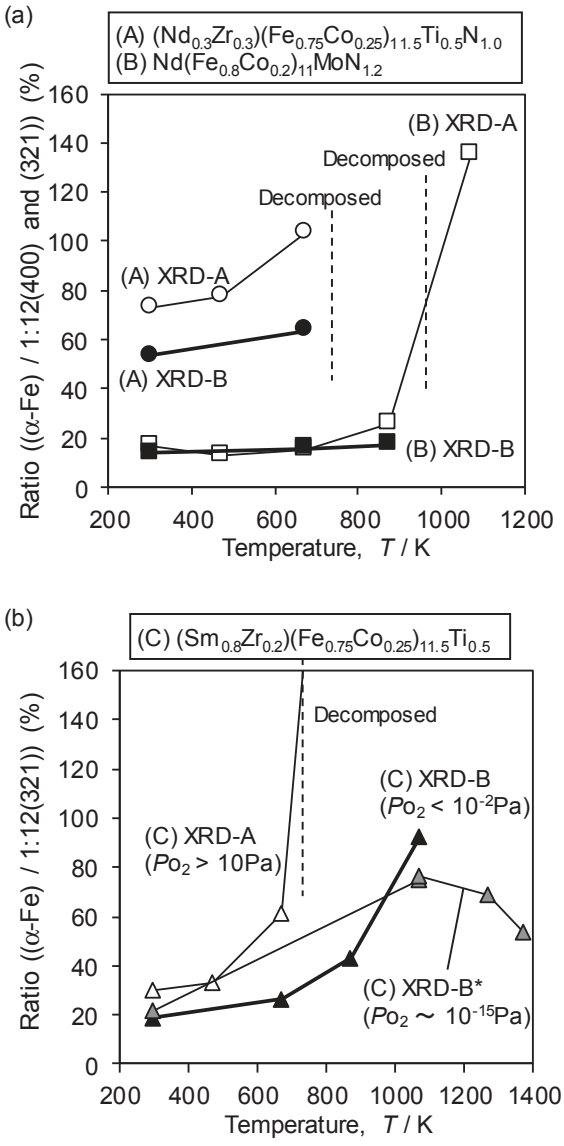

Fig. 6 (a) Variation of intensity ratios of the (110) peak of the α-(Fe, Co) phase to the (321) and (400) peaks of the 1-12 phase in sample (A), and to the (321) peak of the 1-12 phase in sample (B). (b) Variation of intensity ratios of the (110) peak of the α-Fe phase to the (321) peak of the 1-12 phase in sample (C). The XRD-B method was used for all measurements, and the heat-treatment temperatures are shown on the horizontal axis.

phase. Therefore, the XRD patterns obtained by XRD-A can reveal crystal structure information for a deeper portion of the sample particles than those obtained by XRD-B.

As explained for Fig. 1, the two-dimensional surface area of the α-(Fe, Co) phase determined by EBSD is directly related to the volume fraction of the phase.[13] The transfer factor between the values (vol%) based on the EBSD and XRD peak ratios was about 0.3 in this study. In this section, however, we only use the direct peak intensity ratio, $(110)_{Fe}/(400)_{1\text{-}12}$ or $(110)_{Fe}/(321)_{1\text{-}12}$.

Figure 6(a) shows the intensity ratios of the (110) peak of the α-(Fe, Co) phase to the (321) and (400) peaks of the 1-12 phase of sample (A), and to the (321) peak of the 1-12 phase of sample (B). Samples (A) and (B) showed clear exothermic peaks in the DSC curves at around 800 and 1000 K, respectively (Fig. 3). These temperatures corresponded to the decomposition temperatures at which the 1-12 phase peaks disappeared (Fig. 4). The variation in the intensity ratios shown in Fig. 6(a) further supports the decomposition mechanism of the 1-12 structure discussed above.

The peak intensity of the α-(Fe, Co) phase was lower for sample (B) than for sample (A), and the peaks belonging to the $ThMn_{12}$ phase can be observed for sample (B) even after treatment at 1073 K (Fig. 4(b), XRD-A). The origin of these observations was considered to be, first, that the Co Kα X-rays used in XRD-A can detect diffraction from a deeper portion of the sample particles, and second, that the decomposition mechanism is more complex in sample (B) than in sample (A).

The attenuation of the weight increase observed for sample (A) in Fig. 3(c) at 850–950 K almost corresponds to the disappearance of the 1-12 phase diffraction peaks seen in Fig. 4(a). However, the slowdown of the weight increase observed for sample (B) in Fig. 3(c) occurred at 1200–1350 K, which is a clearly higher temperature than that of the disappearance of the 1-12 phase in this sample, which occurred at about 1100 K (Fig. 4(b)). The decomposition of the 1-12 phase is considered to correspond to the loss of nitrogen from this phase, but the slowdown of the weight increase clearly occurred at a higher temperature. Although these observations can be clearly seen in the data shown in Figs. 3 and 4, the details of the decomposition mechanism will require further study.

Figure 6(b) shows that sample (C) decomposed at around 700 K in the XRD-A measurements ($P_{O2} > 10$ Pa). In the XRD-B measurements ($P_{O2} < 10^{-2}$ Pa), however, the 1-12 phase remained up to 1073 K. The intensity ratios of the (110) peak of α-Fe to the (321) peak of the 1-12 phase showed the same behavior, but the ratio of the sample treated at 1273 K for 1 h indicated that the volume fraction of the α-(Fe, Co) phase based on the XRD intensity ratio was about 70% (~23 vol% by EBSD). Therefore, the $ThMn_{12}$ structure remained at 1273 K in the Ar atmosphere with $P_{O2} \approx 10^{-15}$ Pa. Moreover, when sample (C) was heated at 1373 K for 1 h in $P_{O2} \approx 10^{-15}$ Pa, the volume fraction of the α-(Fe, Co) phase decreased to about 17.5 vol% (an XRD intensity ratio of 53%). This observation means that the precipitation of the α-(Fe, Co) phase becomes obvious in the temperature range of 800–1400 K depending on the atmosphere, namely, P_{O2}.

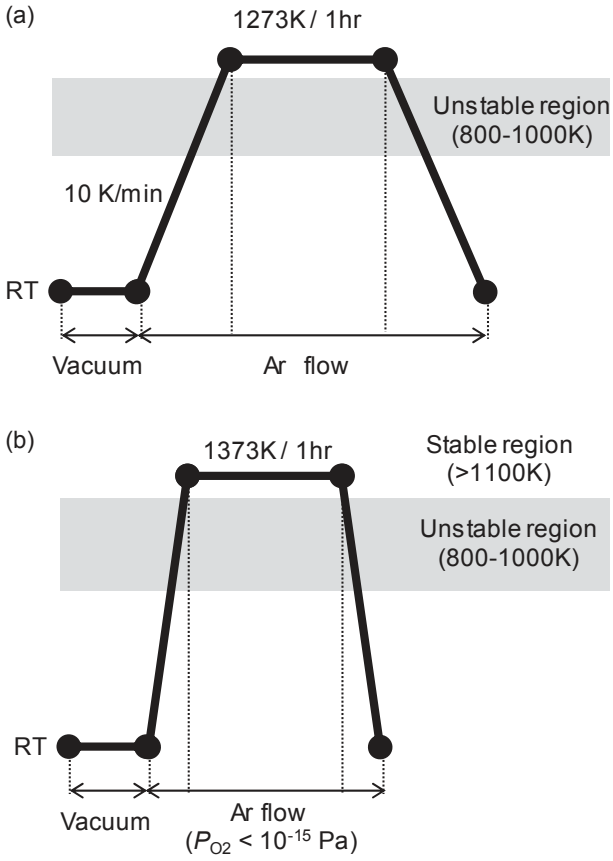

Fig. 7 Schematic representations showing the effects of heat treatment for the (a) 1273 K 1 h Low-P_{O2} and (b) 1373 K 1 h Low-P_{O2} samples.

Figure 7 shows a schematic representation of the above discussion. The precipitated α-(Fe, Co) phase obviously increases from 800 K, as shown in Fig. 4(c) (in the 873 K 1 h pattern). The precipitation clearly decreases in the 1373 K 1 h Low-P_{O2} (~ 10^{-15} Pa) sample. In this study, the starting alloys were annealed at 1373 K before the heat treatment, and the XRD patterns shown in Fig. 4 (RT) are all those of the starting alloys. These showed a limited amount of the α-(Fe, Co) phase, as presented in Table 1, especially in the case of sample (C). Therefore, we consider that the increase of the precipitated α-(Fe, Co) phase appeared during the repeated heat treatments applied in this study, including the effects from oxidation. In conclusion, a harmful temperature region for thermal retreatments is estimated to be 800–1000 K.[11,14] It is assumed that if sample (C) can be subjected to a temperature of more than 1300 K without prolonged exposure to this intermediate-temperature region, the sample should be stable up to its melting temperature.

As shown in Fig. 7(a), heating and cooling sample (C) at the rate of 10 K/min up to 1273 K (in Fig. 5, 1273 K 1 h Low-P_{O2}) led to precipitation of about 23 vol% of the α-(Fe, Co) phase. The duration for which the sample was held at 800–1000 K was estimated to be more than 40 minutes in this case. The observed amount of α-(Fe, Co) phase precipitation (about 23 vol%) was almost the same as that for the other samples treated at 1073 K and 1273 K, as shown in Fig. 5. The precipitation is considered to be due to surface oxidation of the sample particles.

In contrast, the 1373 K 1 h Low-P_{O2} sample shown in Fig. 5(b) was rapidly heat treated at 1373 K by the hand-operation of rapidly insertion and taking out from isothermal zone for heat-treatment (Fig. 7(b)). Therefore, the duration of exposure to a temperature of 800–1000 K was estimated to be very short (less than a few minutes). The precipitated α-(Fe, Co) phase was about 17 vol%, as shown in Fig. 5.

These results demonstrate the existence of effects of passing through the temperature-instability region of 800–1000 K on the decomposition of 1-12 phase for sample (C), except for the oxidation.

At the end of this section, it is worthwhile to mention the Sm vapor pressure of sample (C). In contrast to R = Nd compounds, for R = Sm alloys, such as sample (C), it might be expected that the vapor pressure of Sm plays an important role in the stability of the 1-12 phase and other properties such as the precipitation of the α-(Fe, Co) phase. We examined the origin of the weight gain of sample (C) (Fig. 3(c)) by performing gas analysis to determine the oxygen content and directly measuring the weight gain, and found that the weight gain mainly originates from an increase in oxygen content. Therefore, we conclude that the reduction in the stability of the $ThMn_{12}$ structure in sample (C) can be attributed to (1) sample oxidation and (2) instability of the metastable 1-12 structure in the temperature range of 800–1000 K. Therefore, the direct sublimation of elemental Sm from the sample is almost negligible in the temperature range used in this study.

4. Conclusion

Measurements of the temperature dependence of polarization, DTA-TG, DSC thermal analyses, and XRD patterns of high-temperature-treated samples revealed that the nitrogenated samples (A) $((Nd_{0.7}Zr_{0.3})(Fe_{0.75}Co_{0.25})_{11.5}Ti_{0.5}N_{1.2})$ and (B) $(Nd(Fe_{0.8}Co_{0.2})_{11}Mo_{1.0}N_{1.0})$ started to decompose, that is, to form the α-(Fe, Co) phase and other X-ray amorphous phases, from about 800 and 1000 K, respectively. The non-nitrogenated sample (C) $((Sm_{0.8}Zr_{0.2})(Fe_{0.75}Co_{0.25})_{11.5}Ti_{0.5})$ decomposed above 700 K in a high oxygen partial pressure ($P_{O2} > 10$ Pa), but the main $ThMn_{12}$ structure was still clearly detected up to 1273 K in an almost oxygen-free atmosphere ($P_{O2} < 10^{-15}$ Pa). The recovery of the stability of the 1-12 structure at 1373 K was also confirmed for sample (C).

The $ThMn_{12}$ phase was metastable at RT, and the samples gradually decomposed at 800–1000 K when kept at this temperature for prolonged periods.[11,14] The decomposition of the nitrogenated samples (A) and (B) above 800 and 1000 K, respectively, resulted from the instability of the initial $ThMn_{12}$ structure and the loss of nitrogen from the nitrogenated phase, which was also detected by the TG measurements. For the non-nitrogenated sample (C), the decomposition of the main 1-12 phase was accelerated by the oxidation that occurred under a comparatively high P_{O2} atmosphere as in the high-temperature XRD measurements (XRD-A; $P_{O2} > 10$ Pa). Conversely, the main phase was detected up to about 1273 K in a low P_{O2} of $\sim 10^{-15}$ Pa (XRD-B). Sample (C) was found to be stable in the higher temperature region of 1373–1430 K, as was confirmed by the XRD pattern of a sample treated at 1373 K in a low P_{O2} of $\sim 10^{-15}$ Pa, where the peak intensity of the α-(Fe, Co) phase became weaker than that for the samples treated at lower temperatures. This is a good indication for possibility of preparation of sintered bulk magnets with the sample (C), in the temperature region more than 1373 K up to the melting point.

Acknowledgments

This paper is based on results obtained from the future pioneering program “Developments of magnetic materials technology for high efficiency motors” commissioned by the New Energy and Industrial Technology Development Organization (NEDO).

REFERENCES

1) H.S. Li and J.M.D. Coey: *Handbook of Magnetic Materials vol. 6*, ed. by K.H.J. Buschow, (Elsevier, North Holland, 1991) Chap. 1, pp. 1–83.
2) H. Fujii and H. Sun: *Handbook of Magnetic Materials vol. 9*, ed. by K.H.J. Buschow, (Elsevier, North Holland, 1991) Chap. 3, pp. 303–404.
3) S. Suzuki, T. Kuno, K. Urushibata, K. Kobayashi, N. Sakuma, K. Washio, M. Yano and A. Kato: J. Magn. Magn. Mater. **401** (2016) 259–268.
4) L. Pauling: *The Nature of the Chemical Bond (3rd ed.)*, (Cornell University Press, Ithaca, 1960).
5) T. Kuno, S. Suzuki, K. Urushibata, K. Kobayashi, N. Sakuma, M. Yano, A. Kato and A. Manabe: AIP Adv. **6** (2016) 025221.
6) M. Sagawa, S. Fujimura, N. Togawa, H. Yamamoto and Y. Matsuura: J. Appl. Phys. **55** (1984) 2083–2087.
7) S. Hock: Ph.D. thesis, Dissertation, Universität Stuttgart, (1988).
8) N. Sakuma, S. Suzuki, T. Kuno, K. Urushibata, K. Kobayashi, M. Yano, A. Kato and A. Manabe: AIP Adv. **6** (2016) 056023.
9) K. Kobayashi, S. Suzuki, T. Kuno, K. Urushibata, N. Sakuma, M. Yano, A. Kato and A. Manabe: Proc. REPM2016, (Darmstadt, Germany, 2016) O4-1645, pp. 100–106.
10) K. Kobayashi, S. Suzuki, T. Kuno, K. Urushibata, N. Sakuma, M. Yano, T. Shoji, A. Kato and A. Manabe: J. Alloys Compd. **694** (2017) 914–920.
11) V. Raghavan: J. Phase Equilibria **21** (2000) 464–466.
12) Y. Hirayama, Y.K. Takahashi, S. Hirosawa and K. Hono: Scr. Mater. **138** (2017) 62–65.
13) R.T. Dehoff and F.N. Rhines: *Qualitative Microscopy*, (McGraw-Hill Book Company, New York-street, 1968) p. 291.
14) K. Kobayashi *et al.*: to be proposed to J. Magn. Magn. Mater.